

Noninvasive *in vitro* and *in vivo* assessment of epidermal hyperkeratosis and dermal fibrosis in atopic dermatitis

Jyh-Hong Lee

National Taiwan University Hospital
and
National Taiwan University College of Medicine
Department of Pediatrics
Taipei, 100, Taiwan

Szu-Yu Chen

Che-Hang Yu

National Taiwan University
Graduate Institute of Photonics and Optoelectronics
and Department of Electrical Engineering
Taipei, 106, Taiwan

Shih-Wei Chu

Ten-Chan General Hospital
Department of Dermatology
Chung-Li, 320, Tao-Yuan County, Taiwan

Li-Fang Wang

National Taiwan University Hospital
and
National Taiwan University College of Medicine
Department of Dermatology
Taipei, 100, Taiwan

Chi-Kuang Sun

National Taiwan University
Graduate Institute of Photonics and Optoelectronics
and Department of Electrical Engineering
Taipei, 106, Taiwan
and
Academia Sinica
Research Center for Applied Sciences
Taipei, 115, Taiwan

Bor-Luen Chiang

National Taiwan University Hospital
Department of Pediatrics
and
National Taiwan University College of Medicine
Graduate Institute of Clinical Medicine
Taipei, 100, Taiwan

1 Introduction

Atopic dermatitis (AD) is a chronic inflammatory skin disease associated with cutaneous hyperreactivity to environmental triggers that are innocuous to normal nonatopic individuals.¹

Abstract. Atopic dermatitis (AD) is characterized by hyperkeratosis of epidermis and fibrosis within dermis in chronic skin lesions. Thus far, the histology of skin lesions has been evaluated only by examination of excised specimens. A noninvasive *in vivo* tool is essential to evaluate the histopathological changes during the clinical course of AD. We used Cr:forsterite laser-based multimodality nonlinear microscopy to analyze the endogenous molecular signals, including third-harmonic generation (THG), second-harmonic generation (SHG), and two-photon fluorescence (TPF) from skin lesions in AD. Significant differences in thickness of epidermis and stratum corneum (SC), and modified degrees of fibrosis in dermis (measured by THG signals and SHG signals, respectively), are clearly demonstrated in *in vitro* studies. Increased TPF levels are positively associated with the levels of the THG signals from the SC. Our *in vitro* observations of histological changes are replicated in the *in vivo* studies. These findings were reproducible in skin lesions from human AD. For the first time, we demonstrate the feasibility of preclinical applications of Cr:forsterite laser-based nonlinear microscopy. Our findings suggest that the optical signatures of THG, TPF, and SHG can be used as molecular markers to assess the pathophysiological process of AD and the effects of local treatment. © 2009 Society of Photo-Optical Instrumentation Engineers. [DOI: 10.1117/1.3077182]

Keywords: atopic dermatitis; Cr:forsterite laser; fibrosis; hyperkeratosis; nonlinear microscopy; optical biopsy; second-harmonic generation; third-harmonic generation; two-photon fluorescence.

Paper 08148RR received May 6, 2008; revised manuscript received Nov. 10, 2008; accepted for publication Nov. 18, 2008; published online Feb. 11, 2009.

Various studies indicate that AD has a complex etiology, with activation of multiple immunologic and inflammatory pathways.^{2,3} The biopsy appearances of AD may be indistinguishable from those seen in other dermatitis. However, some histopathological features may sometimes be helpful in making the diagnosis. In chronic AD, characterized by lichenification and dermal fibrotic papules, there is increased hyperplasia and hyperkeratosis (an increased thickness of stratum corneum) of the epidermis. A prominent finding in the licheni-

Address all correspondence to: Dr. Bor-Luen Chiang, Department of Pediatrics, National Taiwan University Hospital, 7 Chung-Shan South Road, Taipei 10002, Taiwan. Tel: 886-2-23123456 ext. 7302; Fax: 886-2-23972031; E-mail address: gicmbor@ntu.edu.tw; or Dr. Chi-Kuang Sun, Graduate Institute of Photonics and Optoelectronics and Department of Electrical Engineering, National Taiwan University, Taipei 10617, Taiwan. Tel: 886-2-33665085; Fax: 886-2-33663614; E-mail address: sun@cc.ee.ntu.edu.tw.

fied plaque is fibrosis of the upper dermis.^{4,5} The observation that chronic AD associated with lichenified plaque, which respond slowly to topical corticosteroids, is somewhat analogous to the recent concerns over the airway remodeling process.^{4,5}

Glimpses through a window into real-life behavior of immune cells are already starting to revolutionize the understanding of the adaptive immune reaction associated with dermatologic diseases.⁶ Intravital microscopy enables investigators to observe the impact of experimental manipulations within any organ or tissue directly *in vivo*.⁷ The two-photon (excitation) fluorescence TP(E)F biopsy of skin based on 780-nm femtosecond (fs) light provides high resolution imaging from the skin surface and their application of Ti:sapphire-based two-photon microscopy (TPM) in human skin *in vivo* has been reported.^{8–10} However, there are several limitations associated with the technique, which include in-focus cell damage and nonlinear phototoxicity.¹¹ Similar to the field of optical coherent tomography,¹² we have recently found that Cr:forsterite fs laser-based systems, with a wavelength around 1230 to 1250 nm, cannot only provide improved penetration capability,¹³ but also significantly increase the embryo viability.^{14–16}

A major challenge for optical sectioning imaging of live specimens is maintaining viability following prolonged exposure to excitation illumination. Chinese hamster ovary cells exposed to two-photon microscopy at 730, 760, and 800 nm remained unaffected at mean power ≤ 1 mW, but were unable to form clones at average power ≥ 2 mW.¹⁷ Hamster embryos were imaged at frequent intervals for 24 h (5 optical sections every 15 min for a total exposure of ≈ 2 J per embryo) using two-photon microscopy at 1047 nm of average laser power 13 mW while maintaining blastocyst, and even fetal, developmental competence.¹⁸ In our previous work observing the cultured mouse oocytes and embryos using harmonic generation microscopy at 1230 nm, after continuous illumination with average power 100 mW (total exposure 29 J per embryo), the embryos were transferred back to the mother mouse. 18 embryos were implanted with 12 mice successfully born (67%), the same ratio as the control group without light exposure.¹⁶ Maximum permissible exposure (MPE) is the level of laser radiation to which an unprotected person may be exposed without adverse biological changes in the skin. According to ANSI Z136.1-2007, the MPE for skin exposure to a laser beam was 1.0×10^{-1} J/cm² for a 1230-nm-based laser, while it was 2.9×10^{-2} J/cm² for a 780-nm-based laser [in terms of surface density of the radiant energy received (radiant exposure) per pulse].¹⁹ Generally, the longer the wavelength, the higher the MPE.²⁰ The single pulse MPE for skin exposure to a 1230-nm laser is 3.45 times that of a 780-nm laser, implying that our technology might be potentially safe and practical in clinical applications. We thus suggest that Cr:forsterite laser-based nonlinear microscopy is an ideal technique for least-invasive assessment of skin samples.^{21,22}

Under the Cr:forsterite fs laser excitation, multiphoton absorption was found to be strongly reduced in most biological specimens, resulting in strongly reduced multiphoton fluorescence signals. Our previous studies have shown that higher harmonic generations could also provide excellent image

contrast.²³ Higher harmonic generations, including second-harmonic generation (SHG) and third-harmonic generation (THG), are virtual-transition-based nonlinear processes and can provide the noninvasive nature desirable for clinical imaging.²³ In contrast to the standard technique of skin biopsies (mechanically removed, sliced, stained, and photographed), optical biopsy using Cr:forsterite laser-based nonlinear microscopy has the advantage of 1. providing a painless technique without skin removal, 2. providing three-dimensional optical biopsies with deep-tissue penetration and subcellular resolution, 3. providing specific optical signature without using exogenous markers, 4. direct access to real-time information under natural physiological conditions *in vivo*, and 5. the feasibility of long-term observations on the same skin area.^{23,24} However, to the best of our knowledge, there are no reports of nonlinear light microscopic imaging of skin lesions of AD *in vivo* and of the feasibility of such clinical applications.

In this study, we have taken advantage of the capacity of Cr:forsterite laser-based multimodality nonlinear microscopy to evaluate the morphological and structural changes of skin lesions of AD in a murine AD model of varying severity induced by epicutaneous sensitization. We also replicated these observations *in vivo*. Finally, optical sectioning images of fixed skin from human AD patients confirmed the reproducibility of our earlier finding from the murine AD model.

2 Materials and Methods

2.1 Mice, Allergens, and Epicutaneous Sensitization

In the *in vivo* study of imaging the mouse ear, nude mice were used as our animal model. The nude mouse is a genetic mutant that suffers from an agenesis of the thymus, and (thus is incapable of mounting most types of immune responses. The skin phenotype of the mouse is that hair shafts fail to penetrate the epidermis, resulting in a lack of body hair. The experimental protocols were performed as previously described.²⁵ In the AD study, 6- to 10-week-old female BALB/c or C57BL/6 mice were obtained from the Animal Center of the College of Medicine, National Taiwan University. AD is associated with increased Th2-type inflammation in acute skin lesions, but chronic AD results from the switching to a Th1-type inflammation.³ It is known that C57BL/6 mice are a strain with a propensity for Th1 responses while BALB/c mice are a strain with a propensity for Th2 responses.²⁶ We use fixed skin of C57BL/6 mice for the evaluation of chronic skin lesions *in vitro*, and observed the fresh skin of the BALB/c mice for the assessment of acute skin lesions *in vivo*. All procedures performed on the mice were approved by The Animal Care and Use Committee of National Taiwan University Hospital. The protein antigens used in this study were ovalbumin (OVA) (100 mg/ml) and staphylococcal enterotoxin (SEB) (0.4 μ g/ μ l) (Sigma Chemical Company, Saint Louis, Missouri). The antigen solution was prepared in distilled water. Epicutaneous (EC) sensitization of mice was performed as previously described.²⁷ In brief, 20 μ L of OVA and 10 μ L of SEB were first added to the paper disk insert of a Finn Chamber (Epitest Company, Tuusula, Finland), and the disk was applied to a 1-cm² patch of sterile gauze, which was then applied to the skin on the lateral side of their abdomen, then fixed and secured with an

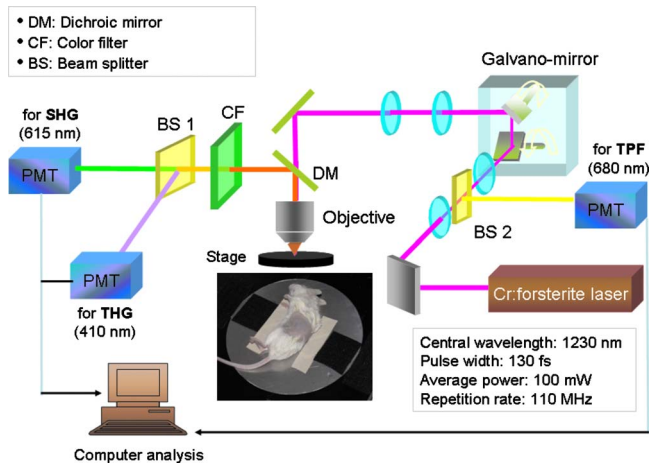


Fig. 1 The experimental setup of the Cr:forsterite laser-based multimodality nonlinear microscopy system. A live mouse mounted on a fixed stage within the microscope ready for acquiring images is shown. A thermal blanket maintaining the body temperature of the test mouse was used during images acquisition. BS, beam splitter; CF, color filter; DM, dichroic mirror; PMT, photomultiplier tube; THG, third-harmonic generation; SHG, second harmonic generation; TPF, two-photon fluorescence. (Color online only.)

elastic bandage to ensure skin contact and to prevent oral ingestion. Three groups of C57BL/6 mice were divided according to the antigen type. Group 1 was OVA group, group 2 was OVA+SEB group, and group 3 was the negative control group with application of phosphate buffered saline (PBS), which was used for comparison. Three mice were used in each group. The courses of immunization were for 5 days.

2.2 Histological Analysis

Skin specimens (lesional skin) obtained from patched areas after the patch was removed at the end of sensitization were used for histological examination. The skin specimens over the other side of the abdomen (nonlesional skin) were also obtained for comparison. Multiple 4-mm punch biopsies were performed, and skin specimens were fixed in 10% formaldehyde overnight, transferred to 30% sucrose, and embedded into optimal cutting temperature (OCT) formulation for frozen horizontal sectioning. The specimens were finally stained with hematoxylin and eosin (HE) for histological analysis. After 10% formaldehyde fixation, some specimens were observed under the stage of microscopy.

2.3 Cr:Forsterite Laser-Based Multimodality Nonlinear Microscopy System

The imaging system used for our experiments was developed in the Ultrafast Optics Laboratory of the Graduate Institute of Photonics and Optoelectronics, National Taiwan University (Fig. 1).^{21,22} The Cr:forsterite laser-based multimodality nonlinear microscopy system was adapted from a FluoView 300 (FV300) scanning unit (Olympus, Tokyo, Japan) combined with a BX51 microscope (Olympus, Tokyo, Japan). The light source was a home-built Cr:forsterite fs laser centered at 1230 nm with a 130-fs pulse width and a 110-MHz repetition rate. The infrared (IR) beam exiting the laser was first shaped by a telescope and then directed into the Olympus

FV300 scanning unit and the Olympus BX51 microscope. Real-time *x-y* scanning was accomplished with a pair of galvanometer mirrors inside the scanning unit. The specimen was mounted on a fixed stage within the microscope. An IR water-immersion objective of working distance 2 mm (LUMplanFL/IR 60×/NA 0.9, Olympus, Tokyo, Japan) was used to focus the laser beam into the observed skin specimen. The average illumination power applied onto the surface of the specimen was 100 mW. Typically, a mean power of 100 mW with a 110-MHz repetition rate was chosen, which corresponds to a pulse energy of 0.91 nJ. For *in vivo* observation, the laser beam exiting the objective was scanned across the specimen, and the backward-propagating multimodal nonlinear signals from the specimen were collected with the same water-immersion objective. The microscope objective employed to focus the laser beam can also act as the collection lens to collect the backward propagation SHG, THG, and multiphoton excited fluorescence. These signals were deflected and discriminated with the 865-nm dichroic mirror (865dxcru, Chroma Technology, Rockingham, Vermont) and transmitted through a color filter (SKG5, CVI Laser optics, Albuquerque, New Mexico), which ensures filtering out the fundamental laser light at 1230-nm wavelength. Different optical harmonic signals were separated with another beamsplitter (BS 1, 490DRXR, Chroma Technology, Rockingham, Vermont). The backward-propagating harmonic signals were detected by different photomultiplier tubes (PMTs) (Harmamatsu R4220P for THG and Harmamatsu R943-02 for SHG, Bridgewater, Westport, Connecticut) with 410- and 615-nm narrowband interference filters (D410/30× and D615/10×, respectively, Chroma Technology) in front, which were synchronized with the galvanometer mirrors. The backward-propagating TPF signals, which were not deflected with dichroic mirrors, were separated with another beamsplitter (BS 2, 865dxcru, Chroma Technology) and detected by another PMT (Harmamatsu R928P). The scanning rate of the FV300 scanning unit was 1000 lines/s corresponding to two frames per second for a 512×512 pixels resolution. Spatial resolution was ≈500 nm and ≈410 nm for SHG and THG signals in the *x-y* plane, respectively. Resolution was on the order of 1 μm in the *x-z* plane.²² Optical observations were made as described.

1. *In vivo* imaging of the nude mouse ear. The nude mouse ear is fixed as previously described.²⁵ The nude mice did not receive any treatment except anaesthetization.

2. Observation of fixed skin specimens from C57BL/6 mice: the skin specimens used were fixed in 10% formaldehyde and were placed on the slide and then on the stage of the microscope. Paired measurements of both the lesional and nonlesional skin respectively of the same mice were performed.

3. *In vivo* imaging of normal and AD skin: BALB/c mice were anesthetized with 150-μl pentobarbital (10 mg/ml) and the hairs of their skin were removed with a hair remover. Objectives were in contact with the skin of the mice, and their interface was rinsed with distilled water. Optical sectioning of *in vivo* mice skin treated with OVA and that of control mice were carried out on the lateral side of their abdomen, which was placed on a special stage suitable for *in vivo* observation.

2.4 Determination of Hyperkeratosis of Epidermis

We measured the x - z -sectioned nonlinear images in fixed skin flaps with intact dermis of C57BL/6 mice. Purple was used as a pseudocolor for the THG signal from SC and epidermis. The skin layers of SC and epidermis were determined as previously described.²¹ Linear lengths of the thicknesses of SC and epidermis on the x - z plane images were determined using ImageJ (National Institutes of Health, Bethesda, Maryland). Five fixed skin flaps were taken from individual mice of each group (control, OVA, and OVA+SEB) to generate a total of 20 x - z plan images for each group.

2.5 Quantitative Analysis of Two-Photo Fluorescence and Third-Harmonic Generation from Epidermis and Second-Harmonic Generation from Dermis

We use the same x - z -sectioned nonlinear images taken from fixed skin samples as described before for quantitative analysis of nonlinear signals. Yellow was used as the pseudocolor for the TPF signal from SC. Green was used as the pseudocolor for the SHG signal from the collagen within the dermis. The skin layers of dermis were determined as previously described.²¹ In brief, the optical sectioning image was saved as uncompressed 8-bit grayscale tiff files and analyzed using the ImageJ software. The signal level was converted to a numerical value using a grayscale from 0 (white) to 255 (black). The background noise was subtracted from all the acquired values. To account for variations in the grayscale intensity due to possible nonuniformity of intact skin tissue, mean gray values (MGVs, average gray value within the region of interest) were measured to determine the levels of TPF and/or THG signals and SHG signals, which reflect the distribution of SC and the distribution of collagen fibers, respectively. The ratio of MGV was defined as: (the MGV of the lesional skin)/(the MGV of the paired nonlesional skin).

2.6 In Vivo Imaging of Murine Atopic Dermatitis Model

To compare the severity of dermal fibrosis of individual BALB/c mice, we acquired stacks of planar projection (x - y plane) images with a depth interval of 1.5 μm starting from the epidermodermal junction at an average depth of $z=30\ \mu\text{m}$ until $z=60\ \mu\text{m}$ from the sample surface *in vivo* from the control and the OVA group, respectively. Serial images at different tissue depths separated by 1.5 μm from individual mice were obtained for analysis. The mean gray value of SHG within the dermis of each planar projection image was determined from three different skin areas of each BALB/c mouse using the same analysis protocol of ImageJ as described before.

2.7 Study of Skin Specimen from Atopic Dermatitis Patients

Skin biopsy was performed from the lesional skin in the left forearm of three female volunteer with AD. After biopsy, the skin specimens were fixed in 10% formaldehyde overnight, transferred to 30% sucrose, and embedded into OCT formulation for frozen horizontal sectioning. The specimens were finally stained with HE for histological analysis. Some samples of specimens after 10% formaldehyde fixation were

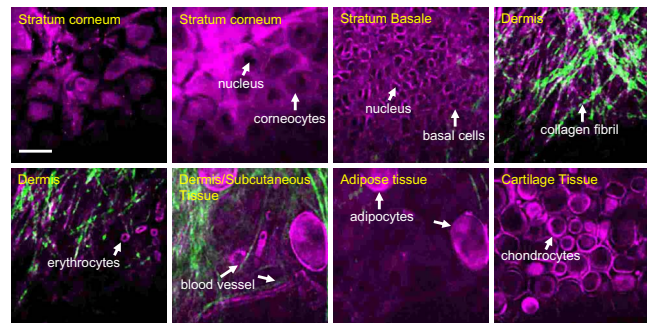


Fig. 2 *In vivo* multimodal x - y plane optical sectioning images at various depths of the ear of a nude mouse. THG signals (purple) reveal morphological features of epidermal tissue layers, subcutaneous tissue (including blood vessel and fat tissue), and the cartilage tissue. The presence of a cartilage tissue layer below the subcutaneous tissue is characteristic of the ear. SHG signals (green) depict the distribution of collagen fibers within dermis. Scale bar: 20 μm . (Color online only.)

observed under the stage of multimodal nonlinear microscopy. Stacks of x - y images with a depth interval of 1.5 μm starting from the skin surface were acquired. The simultaneous mean gray intensity of THG and TPF of serial images were also determined. The Declaration of Helsinki protocols were followed and patients gave their written, informed consent. Our study was approved by the Institutional Review Board of National Taiwan University Hospital.

2.8 Statistical Analysis

Data are expressed as mean \pm standard deviation, unless otherwise specified. The comparison of linear lengths of SC and epidermis and mean gray value among groups were statistically analyzed with a nonparametric Mann-Whitney U test. We compared the mean gray value within the dermis *in vivo* between the control and the OVA group with analysis of variance (ANOVA). Spearman's rank correlation test was used to test for correlation between TPF and THG. All statistical analyses were performed with Prism software (Graph Pad, San Diego, California). A P value of less than 0.05 was considered to indicate a statistically significant difference.

3 Results

3.1 Multimodal Images Depicting Detailed Morphology of Layered Skin Tissues, Subcutaneous Tissues, and Cartilage Tissues in the Nude Mouse Ear In Vivo

THG signals are sensitive to optical inhomogeneities of local tissue,²⁸ hence THG imaging can be used for general morphological assessment. As for SHG, collagen fibrils are known to provide excellent contrast in biological SHG microscopy.²⁹ SHG imaging has recently emerged as a novel approach for studying the pathophysiological remodeling processes of the collagen matrix.³⁰ It is thus highly desirable to take advantage of the least invasive Cr:forsterite fs laser-based multimodality nonlinear microscopy to *in vivo* map morphological features and tissue structures exhibiting nonlinear optical characteristics.

Figure 2 show the representative multimodal x - y plane images acquired at different tissue depths (z) in the ear from the

nude mice *in vivo*. The individual shape of densely packed epidermal cells and transitions between epidermal layers could be clearly resolved through the THG modality. The skin surface of the nude mice reveals the stratum corneum with the typical morphological features of hexagonal shapes of corneocytes. The dark round region exhibiting the nucleus inside the cell body of epidermal cells was easily identified due to the strong THG contrast with laminated organelles,¹⁶ consistent with the observation of neurons and epithelial cell of oral mucosa using THG microscopy.^{31,32} The basal cells are smaller in size compared to the corneocyte. The deeper tissue sections reveal fibrous structures of collagen shown by the SHG signals, which are indicative of the dermis layer. The vascular networks accommodated by the dermis and/or subcutaneous tissue are positively identified through THG by the blood vessels filled with red blood cells (erythrocytes). The adipose tissue or subcutaneous fat composed of adipocytes are clearly revealed by the THG signals with the typically spherical shapes of adipocytes. Below the subcutaneous tissue, THG further observed honeycomb-like structures with hexagonal arrangement. The morphology of this layer is consistent with the structure of cartilage tissue below the dermis. Collectively, each distinct layer of the skin and supporting tissue of nude mouse ear can be clearly resolved by the THG and SHG signals.

3.2 Multimodal Images Revealing Morphological Features of Layered Tissue in the Epidermis and Local Collagen Structures in the Dermis

To determine whether we could identify the histological features in the skin lesions of AD with the Cr:forsterite laser-based multimodality nonlinear microscopy, we induced a murine AD model by epicutaneous sensitization with OVA.²⁷ Multimodal images and emission spectra were acquired for the excitation wavelength λ_{ex} , equivalent to 1230 nm from the excised skin lesions after fixation. Because we aimed to take advantage of the capacity of Cr:forsterite laser-based multimodality nonlinear microscopy to evaluate the morphological and structural changes of skin lesions of AD, we performed the observation only into the depth of dermis (about $z=60$ to $90 \mu\text{m}$). The representative multimodal x - y plane images acquired at different tissue depths (z) into the fixed skin samples from the control and the OVA-treated C57BL/6 mice are shown in Fig. 3(a). We observed many “streaks” of strong THG signals depicting the general morphology of stratum corneum (SC) and epidermal cells. Figure 3(a) also depicts the local aggregations of some fibril that correspond to collagen fibers (for example, $z=60 \mu\text{m}$) through the occurrence of the SHG signals.

A typical emission spectrum acquired from the skin surface is shown in Fig. 3(b). We confirmed the nonlinear signal sources by verifying that the emission spectra of THG signals were with a peak at one third the excitation wavelength (410 nm) and those of SHG signals were with a peak at half the excitation wavelength (615 nm) [Fig. 3(b)]. Some fluorescence signals were noted within SC [$z=0$, Fig. 3(a)]. The fluorescence signals occurred much more frequently in the fixed skin of OVA-treated mice. The two-photon autofluorescence (TPF) signals we observed had a central emission wavelength around 680 nm [Fig. 3(b)].

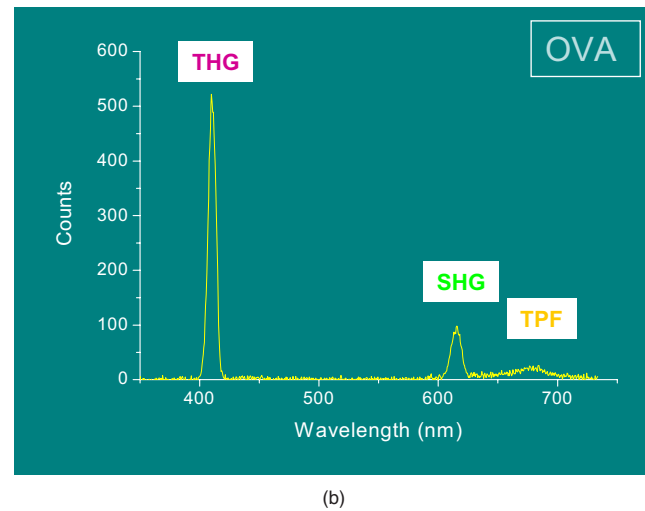
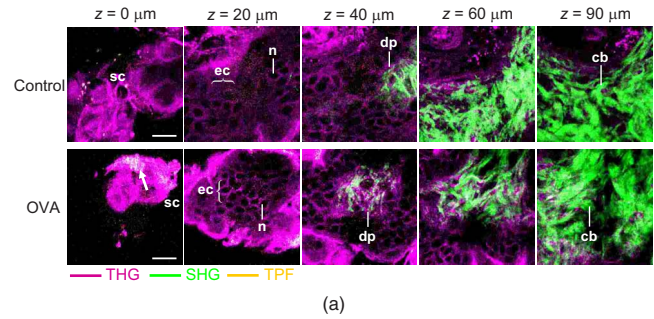


Fig. 3 Multimodal nonlinear images of fixed skin from control and OVA-treated C57BL/6 mice (a) Multimodal optical x - y plane sectioning images at various depths. THG signals (purple) reveal general morphology of SC and shape of densely packed epidermal cells. The dark round region indicates the nucleus inside the cell body of epidermal cells. SHG signals (green) map local aggregations of collagen fibers. Some TPF signals (yellow) within the SC (arrow) were noted in the skin of OVA-treated mice. Scale bar: $20 \mu\text{m}$. Data are representative images of three mice in each group. THG, third-harmonic generation; SHG, second-harmonic generation; TPF, two-photon fluorescence; sc, stratum corneum; ec, epidermal cells; n, nucleus of epidermal cells; dp, dermal papilla; cb, collagen bundle. (b) Emission spectra obtained from the surface ($z=0$) for 1230-nm excitation in the OVA-treated mice. Counts are in arbitrary units. (Color online only.)

3.3 Comparing Optical Sectioning Images to Conventional Microscopic Histology

To ascertain that the histological features observed under the Cr:forsterite laser-based nonlinear microscope were comparable with the conventional histological findings, we compared the nonlinear optically sectioned images with the conventional histologically sectioned images. To evaluate the potential of our nonlinear microscope to assess the histological changes under different disease states, we also introduced another group of murine AD models sensitized to staphylococcal enterotoxin B (SEB), which is known to contribute to the exacerbation of AD.³³ The representative x - z plane images from the fixed skins of three groups of C57BL/6 mice are shown in Fig. 4. These typical pathological changes in the skin lesions of AD can be clearly demonstrated using a conventional microscope [Fig. 4(a)], consistent with the histopathological features reported previously.³⁴ We found that

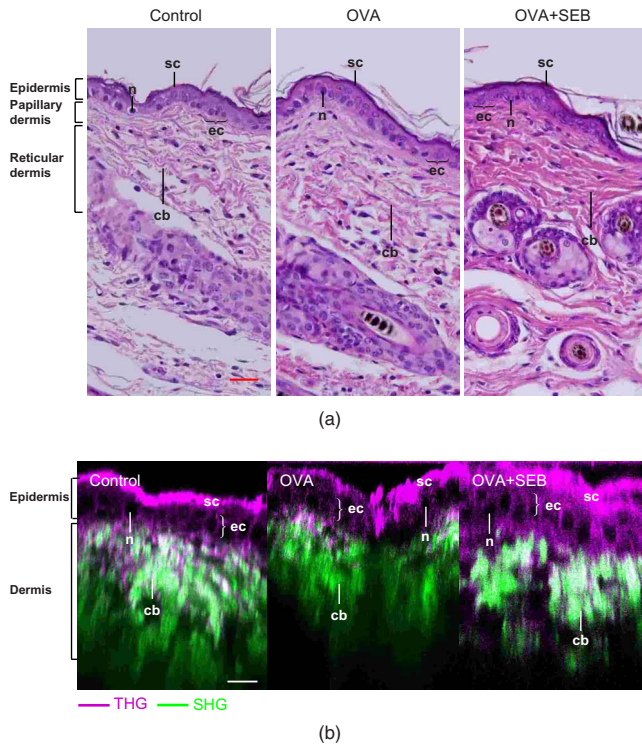


Fig. 4 Comparison of hematoxylin-eosin stained histological images with multimodal nonlinear images of fixed skin from control, OVA-treated mice, and OVA+SEB-treated C57BL/6 mice. (a) Representative H&E-stained histological images of fixed skin including the whole skin layer. (b) Representative multimodal nonlinear x - z plane images of fixed skin. The dark round region indicates the nucleus inside the cell body of epidermal cells. Notice the increased cellular layers within the epidermis of OVA- and OVA+SEB-treated mice groups. sc, stratum corneum; ec, epidermal cells; n, nucleus of epidermal cells; cb, collagen bundle. Scale bar: 20 μm . Data are representative images of three mice in each group. (Color online only.)

sensitization with OVA+SEB induced the most prominent thickening of the SC and epidermis and a remarkable fibrosis in the dermis, indicating a more severe disease status. With the nonlinear microscopy, we observed that after sensitization with OVA+SEB, SC exhibited the strongest THG signals, while dermis displayed considerable local aggregations of collagen fibers depicted through the SHG signals [Fig. 4(b)]. Our results demonstrate similar morphological and structural changes in optically sectioned images of intact skins compared with standard histological images of the same tissue. The epidermis in both treated groups (OVA and OVA+SEB) exhibited multiple cellular layers. It was also noticed that the intensities of the THG signals within the epidermal layers were higher in both treated groups. These findings are also comparable with the histological findings, confirming that the increased cellular infiltration within the epidermis can be readily assessed by THG imaging.

No significant SHG signals were detected in the layers of epidermis, consistent with previous reports.^{10,21} As shown in Fig. 2, SHG mainly reflects the collagen distribution in dermis. Even though THG is contributed from optical inhomogeneity, Fig. 2 also shows that THG signals are strong in stratum corneum, basal cells, red blood cells, the surface of adipocytes, and cartilage tissues. It is thus reasonable to expect

weaker THG signals in the dermis layer, while SHG is a much better modality to identify the collagen matrix distribution. In the x - z images shown in Fig. 4, the THG signals appear dark in the dermis, layer also due to the limited dynamic range of any single image, as the THG intensities in the deeper layer were not normalized according to the signal degradation, which is our case. This dynamic range issue is much less serious when viewing the image in the x - y plane, as shown in Figs. 2 and 3. It is also important to notice that we did not take images deeper than 90 μm from the sample surface. As for signal degradation, there were two main contributions for the THG signal degradation: 1. the collagen fibrils in the dermis are known to be highly scattering and could decrease the detected THG intensity,²² and 2. we had shown that optical signal degradation in the studied human skin specimens is dominated by the distortion-induced broadening of the point spread function (PSF).³⁵ This signal degradation made the SHG/THG signals from the deep layers too weak to show in the same x - z image with the shallow layer due to limited dynamic range of any single image. Even limited by the dynamic range of one x - z image, these unprocessed nonlinear images have enough depth penetration capability for the required analysis.

3.4 Epidermal Hyperkeratosis Revealed by Third-Harmonic Generation Signals

To determine whether we could assess the severity of AD in a quantitative manner, we measured the thickness of epidermis (taken from $z=0$ μm to the epidermodermal junction) and SC from the x - z plane images of fixed skins in lesions of the murine AD models, and compared those with the conventional histological images. A total of 200 measurements (SC and epidermis, respectively) were obtained from each group. For histological sections, results were calculated from 40 conventional HE images at $\times 400$ of each group. We detected significant differences in the thickness of epidermis and SC between three groups using both the nonlinear microscope [Fig. 5(a)] and by using conventional histological methods [Fig. 5(b)] (see Table 1). Sensitization with OVA+SEB induced the greatest thickening of the SC and epidermis.

3.5 Two-Photon Fluorescence Levels Correlate with Third-Harmonic Generation Levels within Thickened Stratum Corneum

Our observation of certain TPF signals within the SC that exhibited markedly prominent THG signals (Fig. 3) led us to conclude that the occurrence of these TPF signals was most likely related to the thickening of SC associated with allergen sensitization. We measured the levels of the TPF signals from the x - z plane nonlinear optical images of fixed skin using ImageJ, and compared them between three groups. A total of 40 measurements were obtained for each group. We found the mean gray intensities of the TPF signals for OVA- and OVA+SEB-treated groups (7.58 ± 1.52 and 8.43 ± 1.48 , respectively) were greater than those of the control group (6.83 ± 1.22), indicating that the intensity of the TPF signals was related to the severity of AD [Fig. 6(a)]. The representative TPF and THG images acquired from x - z and x - y planes of the fixed skin from the three groups are shown in Figs. 6(b)–6(d). We found that TPF imaging is characterized by the

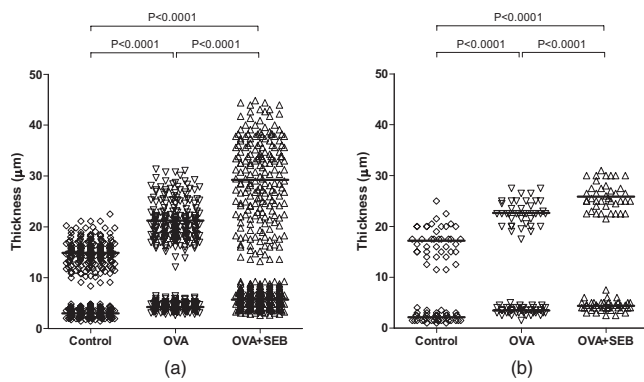


Fig. 5 Determination of the thickness of stratum corneum and epidermis in fixed skin of control, OVA-treated, and OVA+SEB-treated C57BL/6 mice groups using THG signals. (a) Thickness of epidermis and SC obtained by measuring the optical sectioning images in the *x-z* plane. (b) Thickness of epidermis and SC obtained from the conventional histological images. Each data point represents one measurement of the thickness of epidermis and SC, respectively, from control (\diamond), OVA (∇), and OVA+SEB (\triangle) groups. Horizontal lines indicate the mean.

fluorescence pattern within the SC. The TPF signals exhibit diffuse patches of yellow pseudo color in the images of the OVA+SEB-treated mice. Notably, there seemed to be a close correlation between the distribution of TPF signals and THG signals. We then analyzed the magnitude of the TPF and THG signals from the *x-y* plane images acquired at different tissue depths (*z*) into the fixed skin samples using ImageJ. We found a positive correlation between the TPF signals and the THG signals within the control, OVA, and OVA+SEB groups [Figs. 6(b)–6(d)]. Notably, the correlation coefficient (Spearman ρ) of the OVA- and OVA+SEB-treated groups reveals that TPF signals and the THG signals from the SC are more closely correlated than the control groups. Our previous observations confirmed that the general distribution of SC could be revealed by strong THG signals (Fig. 3). Hyperkeratosis is defined by thickening of the skin caused by an increased thickness of the SC.³⁶ We had demonstrated that epicutaneous sensitization with allergens induces thickening of the SC and epidermis (Fig. 5). In lesional skin of AD, there is increased hyperkeratosis of the epidermis, which is less prominent within normal skin tissue. We found the relationships between these two signals are similar in both lesion and normal tissue, but the association is less prominent within normal skin tis-

sue. Collectively, our findings suggest that increased autofluorescence/TPF within the SC is closely associated with the hyperkeratosis of skin (revealed by increased THG signals), which in turn is a manifestation of more severe AD.

3.6 Extent of Dermal Fibrosis Revealed by Increased Second-Harmonic Generation Signals

SHG signal intensity reflects the distribution of connected tissues, composed mainly of type-1 collagen fibers, in the dermis layer.²¹ To determine whether we could assess the severity of AD by quantifying the extent of dermal fibrosis, we measured and compared the intensities of SHG signals from *x-z* plane images of fixed skin from three groups. A total of 100 measurements were obtained from each group. The comparisons of the intensities of SHG signals among the three groups are shown in Figs. 7(a) and 7(b). We found sensitization with OVA+SEB induced the greatest enhancements of SHG signals, implying a direct correlation between the degree of fibrosis and severity of AD. The comparisons of representative *x-y* plane SHG images at *z*=60 μ m from the fixed skin of three different mice are shown in Fig. 7(c). We observed that the collagen fibers in the control group were fine bundles that lie in haphazard arrangement, while in the OVA and OVA+SEB group, the dense bundles of collagen were organized in an interlacing fashion admixed with some hypertrophic collagen fibers [Fig. 7(c)]. Our findings supported that the intensity of the SHG signal is strongly dependent on the collagen fibril thickness.³⁵ The increased distribution of hypertrophic collagen fibers was consistent with our finding that sensitization with allergens induced increased levels of SHG signals.

3.7 *In Vivo* Multimodal Histology of Mice Skin

The high efficiency of the various endogenous nonlinear optical signals (THG, TPF, and SHG) involved show that real-time multimodal imaging lends itself to facile acquisition and analysis of excised tissue in a noninvasive manner. Because most of our analyses were performed *in vitro*, we also sought to test the possibility of the safe application of Cr:forsterite laser-based nonlinear microscopy *in vivo*. To determine whether we could replicate the previous findings on equivalent skin lesions elicited in C57BL/6 mice, we replaced mouse strain C57BL/6 with BALB/c mice and induced AD by sensitization with OVA. We then acquired the serial images at depth intervals of 1.5 μ m from the skin on the abdomen of

Table 1 Measurement of the thickness of epidermis and stratum corneum by histological and optical sections in control, OVA-treated, and OVA+SEB-treated mice group. Mean \pm S.D(μ m), and n=number of measurement.

| | Conventional microscopy histological sections (n=40) | | Multimodal nonlinear microscopy optical sections (n=200) | |
|---------|---|-----------------|---|-----------------|
| | Epidermis | Stratum corneum | Epidermis | Stratum corneum |
| Control | 17.19 \pm 3.05 | 2.13 \pm 0.76 | 14.88 \pm 2.55 | 3.01 \pm 0.71 |
| OVA | 22.66 \pm 2.40 | 3.46 \pm 0.72 | 21.23 \pm 3.94 | 4.24 \pm 0.76 |
| OVA+SEB | 26.65 \pm 3.60 | 4.74 \pm 1.50 | 29.24 \pm 8.14 | 5.70 \pm 1.64 |

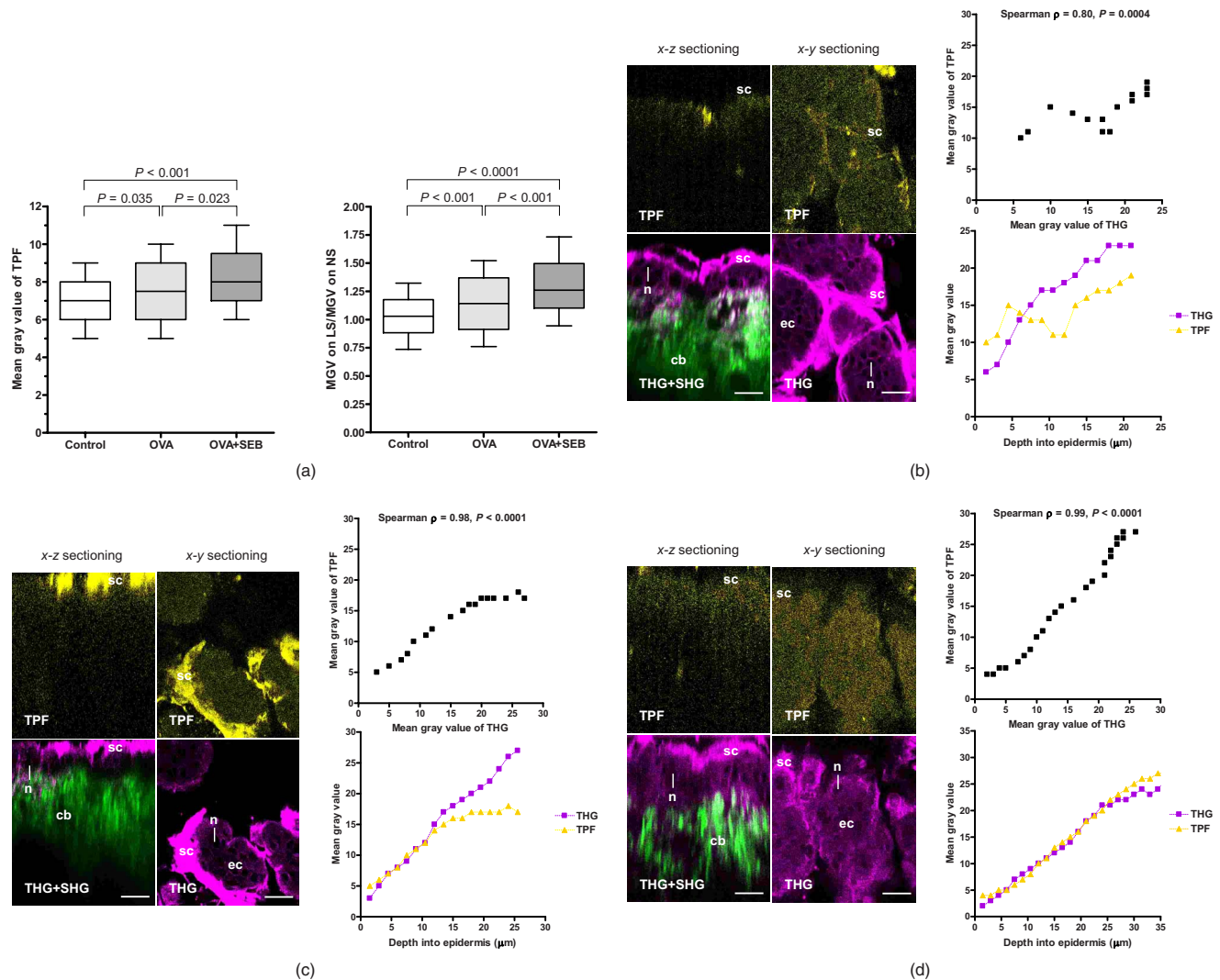


Fig. 6 Correlation between the TPF signal and THG signal in thickened stratum corneum in skin lesions of murine AD models. We measured the intensity levels of TPF and THG signals by determining the mean gray value (MGV) of optical sectioning images (8-bit grayscale tiff files) of the fixed skin from three groups. (a) Comparison of MGV of the TPF signals on fixed lesional skin (left) and ratio of the MGV of TPF on fixed lesional skin (LS) to that on fixed nonlesional skin (NS) (right). The box extends from the 25th percentile to the 75th percentile of all measurements. Horizontal line indicates the median. (b), (c), and (d) Simultaneous TPF and THG+SHG images from *x-z* and *x-y* planes of fixed skin from mice of (b) control, (c) OVA-treated, and (d) OVA+SEB-treated (d) C57BL/6 mice. The relationships between the mean gray value of TPF and that of THG on the same optical sectioning image at different tissue depths of epidermis were analyzed by Spearman correlation coefficient (ρ), and the trends of change between the mean gray value of TPF and that of THG with increasing tissue depth of epidermis is shown. sc, stratum corneum; ec, epidermal cells; n, nucleus of epidermal cells; cb, collagen bundle. Scale bar: 20 μm . (Color online only.)

anesthetized mice using nonlinear microscopy *in vivo*. *In vivo* movies of stacks of *x-y* plane images in mice skin from control and OVA-treated groups were obtained (supplementary files: Videos 1 and 2, respectively). We observed the same histological morphology of epidermis and structural details of dermis as that of *in vitro* experiments in each group. Some strong fluorescence signals were noted within the SC of the epidermis from the OVA-treated group, but not within the control ones. We measured the levels of the TPF signals using ImageJ and compared them between control and OVA-treated groups. Again, we found the mean gray intensities of the TPF signals for OVA-treated groups were significantly greater than those of the control group (14.13 ± 1.48 versus 7.04 ± 0.54 , $P < 0.0001$), indicating that the intensity of the TPF signals

was related to AD *in vivo*. Moreover, to determine whether we could evaluate the serial changes of dermal fibrosis at different tissue depths of dermis, we measured the intensities of SHG signals from *x-y* plane images of skin lesions from both mice groups *in vivo*. We found that the changes in the intensities of SHG acquired from the epidermodermal junctions of three different skin areas of individual mice were significantly different between control and OVA-treated groups [Fig. 8(a)]. The representative serial *x-y* plane images at different depths are shown in Fig. 8(b), indicating that the increased intensities of SHG signals were directly proportional to increased amounts of dense collagen fibers at various tissue depths of the dermis of OVA-sensitized mice. Representative H and E-stained histological images of *x-y* planes at various depths

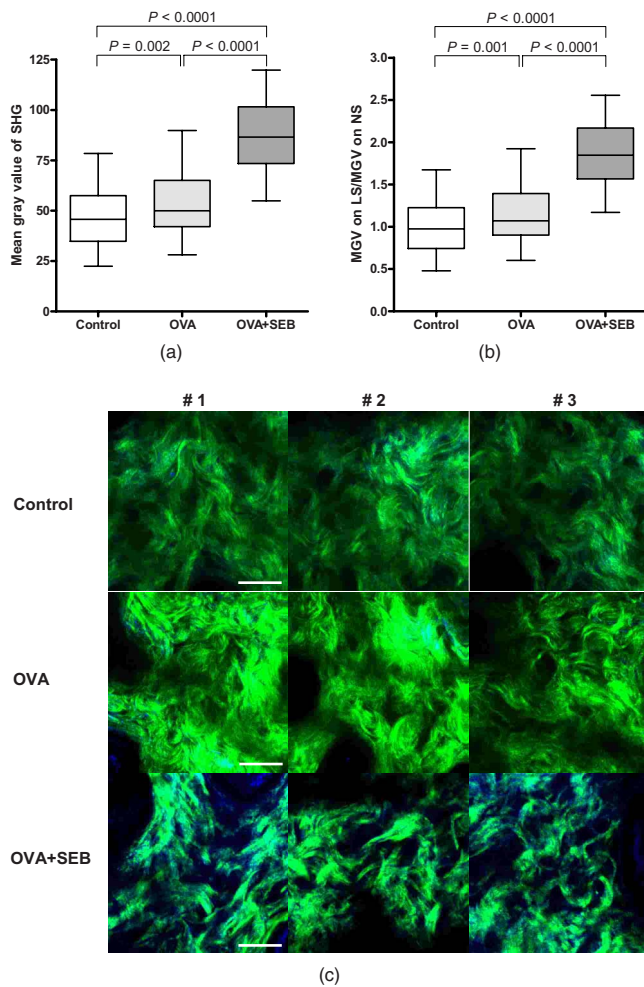
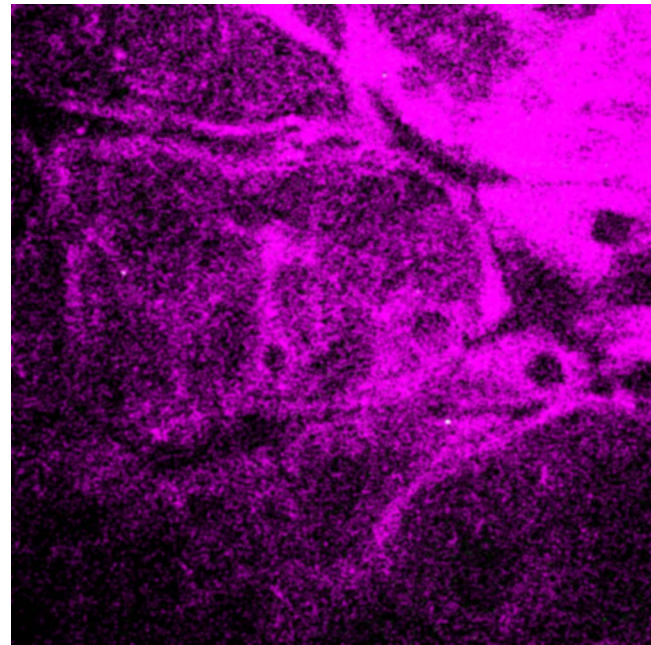


Fig. 7 Correlation between SHG intensities and the extent of fibrosis in fixed skin of control, OVA-treated mice, and OVA+SEB-treated C57BL/6 mice group. We measured the intensities of SHG signals by determining the mean gray value (MGV) of optical sectioning images (8-bit grayscale tiff files) from the x - z plane of fixed skin from three groups. (a) Comparison of MGV of SHG on fixed lesional skin and (b) ratio of the MGV of SHG on fixed lesional skin (LS) to that on fixed nonlesional skin (NS). The box extends from the 25th percentile to the 75th percentile of all measurements. Horizontal line indicates the median. (c) Representative x - y plane SHG images of fixed skin from control, OVA-treated mice, and OVA+SEB-treated C57BL/6 mice group. SHG signals (green) map different distribution patterns of collagen fibers. The dense collagen fibers organize in interlacing fashion in the OVA group, while hypertrophic collagen bundles display aggregated structure in the OVA+SEB groups. The number (#) indicates different individual mice. Scale bar: 20 μm . Data are representative images of each of three mice in each group. (Color online only.)

of fixed skin confirmed that the dense bundles of collagen were organized in an interlacing fashion in the OVA-treated group [Fig. 8(c)].

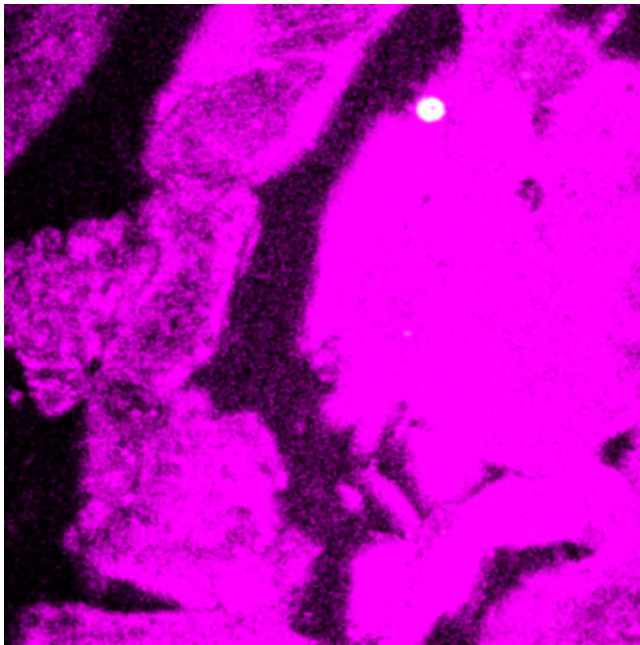
3.8 Preclinical Application in Atopic Dermatitis Patients

To ensure the reproducibility of our previous findings in a murine AD model, optical sectioning images of fixed skin from human AD patients were acquired. We included one female volunteer who was 26 years old and diagnosed with AD



Video 1 *In vivo* movies of depth-resolved x - y plane sectioning images from the abdominal skin of control BALB/c mice. THG signals in purple pseudocolors reveal the general morphology of SC and epidermis. SHG signals in green pseudocolors map local aggregations of collagen fibers within dermis. The optical depth difference between adjacent images is 1.5 μm . Image size: $80 \times 80 \mu\text{m}$. Video is representative of three mice (QuickTime, 3 MB). [URL: <http://dx.doi.org/10.1117/1.3077182.1>]

for 3 years, and who provided a biopsy specimen from the AD lesion over her left forearm extensor side. The representative optical sectioning and conventional histological images from the x - z plane are shown in Fig. 9(a). We observed that increased THG signals reflect the markedly thickened SC, which corresponds to epidermal hyperkeratosis in the HE staining image [Fig. 9(a)]. The thickness of the SC in the female forearm was found to be 10 to 15 μm .¹⁰ Both types of images showed that the thickness of the SC in the forearm of the female patient with AD was around 20 to 40 μm , supporting the fact that increased thickness of SC (hyperkeratosis) is a characteristic feature of chronic AD.⁴ These data also illustrate that the feasibility of determining epidermal thickness and SC in human AD studies using nonlinear microscopy is comparable to that of conventional microscopy. The representative THG-SHG x - y plane images acquired at different tissue depths (z) in the fixed skin sample are shown in Fig. 9(b). We observed that serial changes in the morphological features of SC, stratum spinosum, and stratum basale could be clearly recognized. Additionally, we observed increased TPF within the thickened THG signal representing SC [Fig. 9(a)]. The dark round region indicates the nucleus inside the cell body of epidermal cells due to the strong THG contrast with laminated organelles.¹⁶ We validated the nonlinear signal origins by verifying that the emission spectra of THG, SHG, and TPF were centered at 410, 615, and 680 nm, respectively [Fig. 9(c)]. We tried to verify the origin of TPF by measuring the emission spectrum acquired from pure human keratin solution (K0253, Sigma Aldrich), but no measurable fluorescence from pure keratin solution was detected. Many protein



Video 2 *In vivo* movies of depth-resolved *x-y* plane sectioning images from the abdominal skin of OVA-treated BALB/c mice. In comparison with Video 1, thickened SC of epidermis and hypertrophic collagen fibers within dermis were clearly demonstrated. Note that the bright spot (yellow pseudocolor) in the right upper field indicates the occurrence of two-photon autofluorescence (TPF) signals within the thickened SC. The optical depth difference between adjacent images is 1.5 μm . Image size: 80 \times 80 μm . Video is representative of three mice (QuickTime, 2 MB). [URL: <http://dx.doi.org/10.1117/1.3077182.2>]

molecules are expressed in particular locations in the SC.³⁶ Our results indicated that the measured TPF might be contributed from other endogenous molecules associated with the process of keratinization/hyperkeratosis.

To investigate the possible association of TPF with hyperkeratosis, we further enrolled two additional female volunteers who were 18 [Figs. 10(a)–10(c)] and 16 years old [Figs. 10(d), 10(e), and 10(f)], respectively. The representative simultaneous THG and TPF images acquired from the *x-y* plane of the same position of fixed skin are shown in Figs. 10(a) and 10(d), respectively. We found an excellent correlation between the localization and distribution of THG and TPF signals. We then applied the same analysis technique as in the murine AD model for assessing the intensities of TPF and THG signals from *x-y* plane images. We found significantly positive correlations between the intensities of TPF and THG signals from the fixed skin of the two AD patients [Figs. 10(b), 10(c), 10(e), and 10(f)]. Thus we were able to show that the changes in TPF intensity with hyperkeratosis in the skin lesion of AD patients in humans are compatible with our mouse model studies.

4 Discussion

We have demonstrated the feasibility of the application of Cr:forsterite fs laser-based multimodality nonlinear microscopy in *in vitro* and *in vivo* imaging of skin lesions of AD. This study clearly demonstrates that the histological changes in the skin lesions of AD can be quantitatively assessed in a

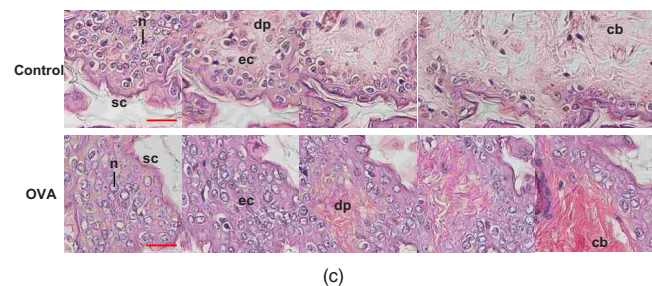
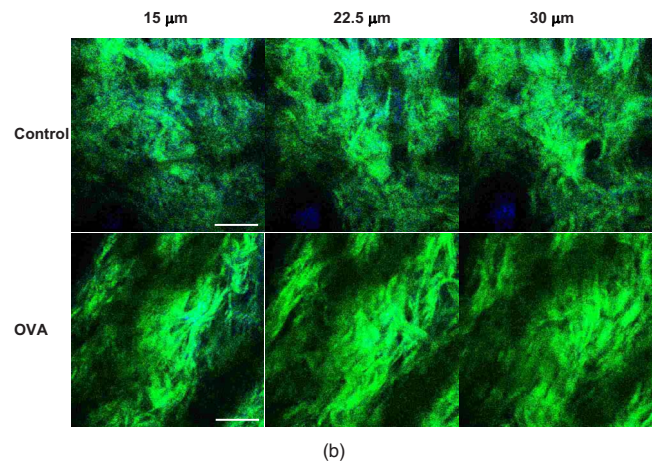
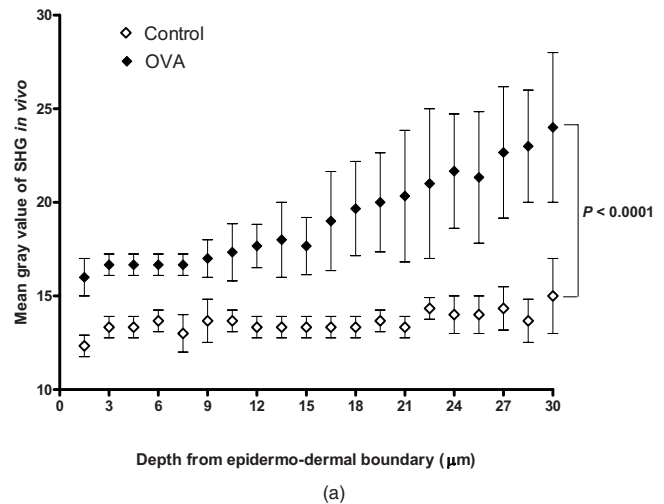
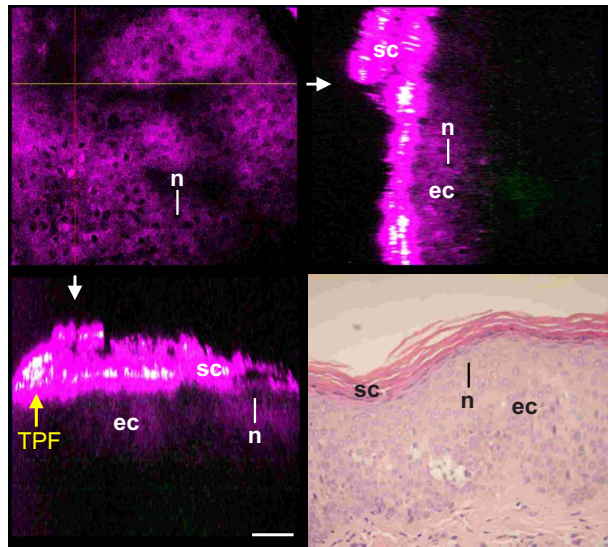
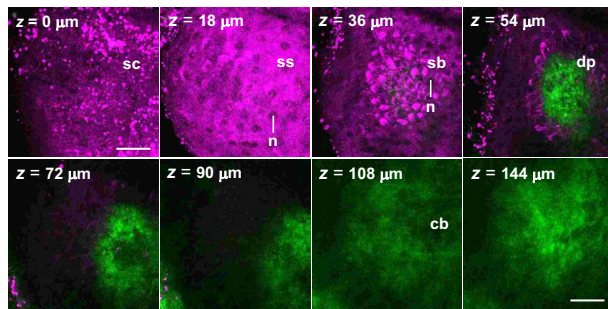


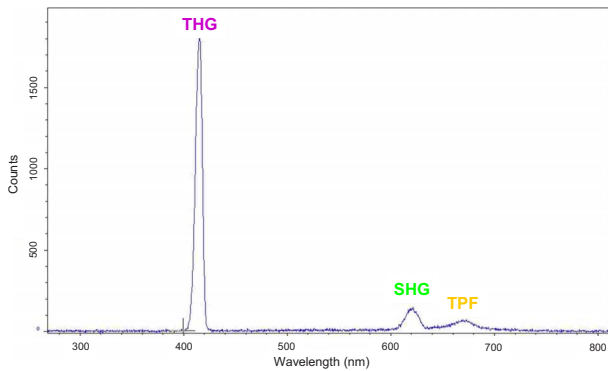
Fig. 8 *In vivo* assessment of dermal fibrosis in individual BALB/c mice. (a) The change of dermal fibrosis represented by the increased mean gray intensity of SHG from dermis of individual mice. The mean gray value of SHG was measured from *x-y* plane images from three different abdominal skins of individual mice *in vivo*. Values are mean \pm SD. The comparisons between control and OVA-treated BALB/c mice groups were analyzed by ANOVA. (b) Three representative SHG images at depths of 15, 22.5, and 30 μm from the epidermo-dermal junction, respectively, from both groups. In the OVA group, the amounts of collagen fibers (represent by SHG signal in green) increase proportionately with the tissue depth of dermis. Scale bar: 20 μm . Data are representative of three mice in each group. (c) Representative HE-stained histological images of *x-y* plane at various depths of fixed skin from control and OVA-treated BALB/c mice. sc, stratum corneum; ec, epidermal cells; n, nucleus of epidermal cells; dp, dermal papilla; cb, collagen bundle. (Color online only.)



(a)

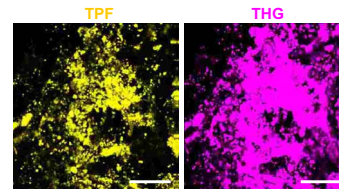


(b)

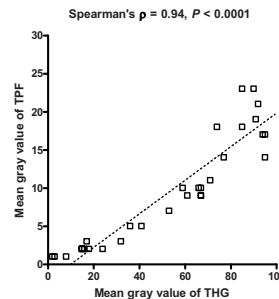


(c)

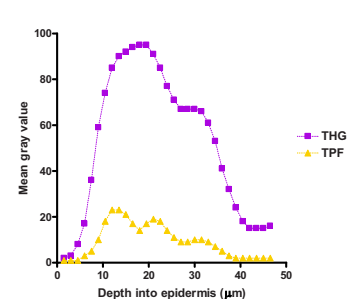
Fig. 9 Comparison of optical sectioning image with HE-stained histological images of fixed skin lesions from an AD patient. (a) The optical nonlinear sectioning image from two different x-z planes are shown (white arrow). The morphological features of SC in the epidermis are clearly demonstrated by THG signals in purple pseudocolor. The dark round region indicates the nucleus inside the cell body of epidermal cells. The autofluorescence is located within the thickened SC (yellow arrow). (b) Serial x-y plane optical sectioning images from fixed skin lesions of an AD patient. THG signals (purple) reveal general morphology of SC and transitions between epidermal layers; SHG signals (green) map local aggregations of collagen fibers. sc, stratum corneum; ss, stratum spinosum; sb, stratum basale; ec, epidermal cells; n, nucleus of epidermal cells; dp, dermal papilla; cb, collagen bundle. Scale bar: 20 μm . (c) Emission spectra obtained from the surface ($z = 0$) of fixed skin from an AD patient for 1230-nm excitation in an AD patient. Counts were in arbitrary unit. (Color online only.)



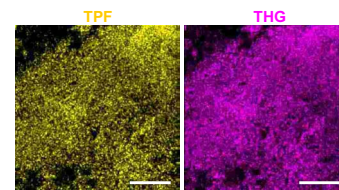
(a)



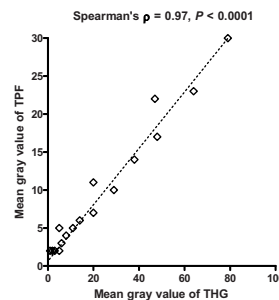
(b)



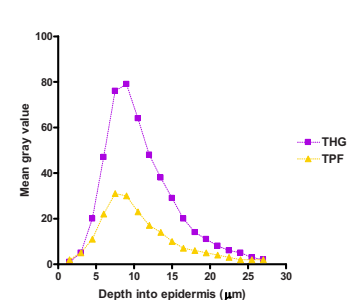
(c)



(d)



(e)



(f)

Fig. 10 Increase in intensity of TPF signal within the thickened stratum corneum in skin lesions of AD patients. (a) and (d) Simultaneous x-y plane TPF and THG images of fixed skin from two AD patients. (b) and (e) Correlation between the mean gray value of TPF with that of THG analyzed by Spearman correlation coefficient (ρ). (c) and (f) Trends of change between the mean gray value of TPF and that of THG with increasing tissue depth of epidermis. Scale bar: 20 μm . (Color online only.)

least-invasive manner. The morphological changes (thickness of epidermis and SC) in the epidermis can be measured by the THG signal, while the structural changes of local connective tissue (contents of collagen and extent of fibrosis) in the dermis can be quantified by the SHG signal. The endogenous autofluorescence of skin was associated with the epidermal hyperkeratosis in AD. Additionally, we have verified the pre-clinical efficacy of the *in vivo* application of Cr:forsterite fs laser-based nonlinear microscopy in human studies.

We have previously reported the application of optical biopsies of fixed mouse skin and fixed human skin.^{21,22} The

Table 2 The comparison of different optical biopsy technology on their application of inflammatory dermatitis.

| Technology | Evaluation parameters | Resolution/penetration depth | Technical comments (advantages/disadvantages) | Reference |
|---|---|--|---|-------------------------|
| <i>Optical coherence tomography</i> | Epidermal thickness; thickened and/or disrupted entrance signals; reduction of dermal reflectivity | 8 μm axially and 10 μm laterally/about 1 to 2 mm | Advantages: deeper penetration depth, wider field of view, and vertical cross sectional imaging. Disadvantages: cannot detect substances that do not scatter; cannot detect horizontal cross section; lesser resolution; layered-skin structure. | 37–39 |
| <i>Reflectance confocal microscopy</i> | Stratum corneum disruption, spongiosis, exocytosis, vesicle formation, and epidermal thickness. | 3 to 5 μm axially and 0.5 to 1 μm laterally/300 to 400 μm | Advantages: horizontal cross section; change the depth of imaging; high resolution morphology. Disadvantages: depth of imaging limited to superficial dermis; grayscale contrast lacks specificity. | 40–42 |
| <i>Ti:sapphire laser-based two-photon excitation fluorescence microscopy</i> | Individual cells, skin structures, intracellular components, connective tissue structure, TP(E)F, SHG | 1 to 2 μm axially and 0.4 μm laterally/maximum 500 μm | Advantages: high optical resolution; functional autofluorescence imaging from endogenous fluorophores and protein structures. Disadvantages: photodamage, photobleaching, limited penetration depth, lack of THG signal. | 10, 24, and 43 |
| <i>Cr:forsterite laser-based nonlinear microscopy (higher harmonic generation microscopy)</i> | Thickness of epidermis and SC by THG, fibrosis in dermis by SHG, hyperkeratosis by TP(E)F | 1 μm axially and 0.4 to 0.5 μm laterally/maximum 1.5 mm | Advantages: multimodal signals including SHG, THG, TP(E)F; high optical resolution; lack of energy deposition. Disadvantages: much reduced autofluorescence from endogenous fluorophore. | 21 and 22 present study |

present study takes it a step further and demonstrates the *in vitro* and *in vivo* imaging of skin lesion from the murine AD model and the *in vitro* imaging of skin lesions from AD patients for the first time. The skin structure can be measured by using other techniques, such as optical coherence tomography (OCT),^{37–39} reflection confocal microscopy,^{40–42} and Ti:sapphire laser-based TPF microscopy.^{10,24,43} The advantages/disadvantages of our technology over the competing techniques are summarized in Table 2. Because the penetration capacity and imaging depth of different specimens could be drastically different, we focus the comparison of different technology on their application of inflammatory dermatitis. With the aid of a Cr:forsterite fs laser-based nonlinear microscope, the morphological features of layered tissue and local collagen structures in skin lesions can be quantitatively evaluated using computer-based image analysis. The THG images shown in all figures do have adequate optical sectioning capability to identify the nuclear size/shape and to map morphological features and tissue structures. The technique could prove to be a valuable tool in the diagnosis or long-term follow up of the skin of patients by directly assessing the real-

time pathophysiological information *in vivo*. Development of clinical applications of this technique in studying patients with AD and other human dermatological disorders can be expected in the future.

At present, the lack of universal methods for fluorescent labeling of living tissues is a major obstacle in two-photon tissue imaging.⁴³ Even though a suitable mAb is available, with the strong autofluorescence emitted from the endogenous fluorophores of skin, fluorescence conjugated mAb could no longer be distinguished due to the overlapping autofluorescence.⁴⁴ Oxidative photodamage can be caused by two- or higher-photon excitation processes of endogenous fluorophores, such as Flavin-containing oxidases.⁴³ Additionally, inside a highly scattering specimen such as human skin, the contrast of autofluorescence images is significantly degraded at the depth of 200 to 300 μm .⁴³ The Cr:forsterite fs laser does have same limitations, because multiphoton absorption was found to be strongly reduced in most biological specimens, resulting in strongly reduced multiphoton fluorescence signals.⁴⁵ Our technology cannot take advantage of en-

ogenous fluorophores, such as reduced nicotinamide adenine dinucleotide phosphate (NADPH) and flavin adenine dinucleotide (FAD), because the diagnostic information produced by such fluorescent biomolecules is missing. However, our recent studies on commonly used bioprobes indicated efficient multiphoton fluorescence from a lot of bioprobes excited with 1230-nm Cr:forsterite laser light.⁴⁶ Additionally, THG microscopy can be utilized as a general-purpose microscopy technique for morphological studies, which is not available with Ti:sapphire lasers. By using a multimodal nonlinear microscope and using exogenous fluorophores conjugated to mAb, the entire visible spectrum and NIR regions are open for fluorescence detection, which are desirable multiphoton fluorescence left for molecular imaging with high specificity. Harmonic generation signals thus can be used for noninvasive structure imaging, and can be combined with minimized multiphoton fluorescence for universal methods for fluorescent labeling of live cells and tissues.

It is generally known that photodamage in the focal plane is primarily due to two-photon excitation (TPE) processes. Phototoxicity and compromised viability may be especially pronounced at the shorter Ti:sapphire wavelengths where multiphoton absorption of intrinsic tissue chromophores is high.⁴⁷ Higher harmonic generations (HHG), including SHG and THG, are known to leave no energy deposition to the interacted matters due to their virtual energy conservation characteristic; that is, the emitted HHG photon energy is the same as the total absorbed excitation photon energy, thus relatively little local heat is produced.²³ Recent studies have suggested that the lowest light attenuation (including absorption and scattering) in most biological materials exists around 1200 to 1250 nm,⁴⁸ which is not available with the Ti:sapphire lasers. In contrast to Ti:sapphire fs laser excitation, multiphoton absorption of Cr:forsterite lasers is strongly reduced with a longer 1230-nm light. Although the average excitation power (100 mW) on sample is higher than the typical excitation power (<10 mW) in two-photon microscopy using a Ti:sapphire laser as an excitation source, from Figs. 3(b) and 9(c), the counts of TPF signal emitted from the SC are about 20 times smaller than those of the THG signal. On the other hand, a fair comparison in phototoxicity should be based on the sample viability where the quality [signal-to-noise ratio (SNR)] of nonlinear signals excited by both lasers is at the same level. The ultimate comparison in phototoxicity thus is based on the penetration capacity with the comparable SNR. In our previous study of human skin,²² we were able to observe the dermis structure with a depth of more than 400 μm using Cr:forsterite lasers (1230 nm) with excitation power of 100 mW, while that of Ti:sapphire lasers-based nonlinear microscopy can only get down to a depth of 200 μm using Ti:sapphire lasers (750 nm) with excitation power of 20 mW.¹⁰ Desirable quality (SNR) of nonlinear signals in optical section imaging from the more deeper tissue-layered structures, achieved by our system, combined with previous experimental studies on embryo viability, show that a 150-mW Cr:forsterite laser^{16,23} has a much higher viability than a 2-mW-Ti:sapphire laser.¹⁷ The intrinsic nonlinearity of higher harmonic generation provides the optical sectioning capability, while the selected 1230-nm near-infrared light

source provides the deep-penetration capacity and enhanced viability.

Keratinization is a complex differentiation process.³⁶ The SC, composed of keratinized dead cells (cornified cell), is a laminated composite structure with distinct protein “bricks” (cornified cell) embedded in a lipid multilayer “mortar” matrix.⁴⁹ Structurally, these are organized into lamellar multilayers with lateral arrangement. The internal side of a cornified cell is a keratin-rich fibrous matrix that occupies the entire intracellular volume. The lipid multilayer is comprised of fatty acid, ceramide, and cholesterol.³⁶ From the highly correlated images of the thickened SC revealed by the TPF and THG signals, we suggest that the TPF and THG modalities might share common sources of origin derived from the hyperkeratosis (increased keratinization process) of the SC in more severe AD in human and mouse skin. It has been reported that keratin is a major contributor to autofluorescence signals in the epidermis on the basis of histological localization,^{50,51} and that hyperkeratotic lesions were identifiable by a strong fluorescence from the keratin layer.⁵² However, no fluorescence from pure keratin solution was detected in our study. Additionally, many molecules, such as loricrin, profilaggrin, trichohyalin, involucrin, SPRs, and S100A, are expressed in particular locations in the SC.³⁶ Thus the contribution of other endogenous molecules should also be considered. As for the origin of THG, a THG is observed in the lamellar structure of effective refractive index and lamellar inhomogeneities in the studied sample,⁵³ and the surfactant lamella body, revealed by THG, had been reported.⁵⁴ Emission spectral characteristics were found to be associated with the intercellular lipid (mainly ceramides) bilayers and lamellar granule in the SC.⁵¹ Comparing images based on THG and TPF signals, we can confirm both biophysical origins of THG and TPF signals located within the SC of epidermis. But the exact signal contrast might be different because of the complex process of keratinization. We speculated that in the thickened SC associated with AD, the higher TPFs originate mainly from the complex protein matrix formation, while the accumulated lamellar multilayers are responsible for the increased THG signal.

In the *in vitro* study of C57BL/6 mice, the mean gray intensities of the TPF signals for OVA-treated groups were significantly greater than those of the control group (7.58 ± 1.52 versus 6.83 ± 1.22 , $P=0.035$). In our *in vivo* study of BALB/c mice, under which circumstance there was no fixation process of the skin specimens, strong fluorescence signals were still noted within SC of the epidermis from the OVA-treated group, but not within the control group (14.13 ± 1.48 versus 7.04 ± 0.54 , $P < 0.001$). It is interesting to find that the mean TPF signals are similar between the two control groups from *in vitro* C57BL/6 mice (6.83 ± 1.22) and from *in vivo* BALB/c mice (7.04 ± 0.54). Furthermore, the mean TPF signals in the *in vivo* BALB/c mice (14.13 ± 1.48) are greater than that of *in vitro* C57BL/6 mice (7.58 ± 1.52). This TPF discrepancy reflects the difference in biophysical properties of SC between the live and dead skin lesions of AD, hence the different intensities in the autofluorescence. Although many articles reported that the tissue fixation changes the fluorescence characteristics, it is reasonable that

fixation artifacts are not applicable to our observed difference between AD and control groups.

It is well known that chronic skin lesions of AD are characterized by thickened plaques with increased lichenification and dry, fibrotic papules.¹ With further lichenification of the lesions, there is prominent hyperkeratosis in the epidermis and some vertical streaking of collagen in the papillary dermis.⁵⁵ The lichenification and dermal fibrosis respond slowly to topical corticosteroids.⁴ It is therefore mandatory to monitor such chronic changes repeatedly after long-term treatment has been initiated. Thus far, the composition of dermal matrix has been evaluated only by histological examination of excised skin specimens. The conventional microscopic images of the HE-stained histological sectioning of the sample are gold standard for the purpose of revealing these histopathological features. The use of multiphoton microscopy in the noninvasive, spatially localized *in vivo* characterization of cell–extracellular matrix (ECM) interactions in unstained thick tissues has also been reported.⁵⁶ Our present study further demonstrates that Cr:forsterite fs laser-based nonlinear microscopy is a novel approach for studying the pathophysiological remodeling process of the collagen matrix in AD. We could quantitatively evaluate alterations in collagen in the dermis *in vivo* in a noninvasive way and monitor the outcome of dermal fibrosis during topical steroid therapy. We think depth-resolved signal analysis is part of quantitative approaches that were not informative enough compared to the histopathological imaging approach. We suggest that both the increased SC thickness revealed by THG and the increased dermal fibrosis revealed by SHG are the most important parameters for the long-term follow up of therapeutic effects using the optical sectioning method. Furthermore, endogenous skin autofluorescence can serve as a quantitative marker for assessing hyperkeratosis associated with the epidermal changes associated with AD.

A number of different murine models of AD have been reported.⁵⁷ The currently reported mouse models of AD can be classified into four different categories; one of them is AD-like skin lesions induced by protein sensitization. AD can be induced by epicutaneous sensitization with chicken OVA in protocols described by Spergel et al. and Wang et al. (our model), both models displaying many of the features of human AD.^{26,34} Our model shows the most important aspects of AD, i.e., characteristic skin lesions compatible with the typical histopathology of typical AD. We have replicated equivalent skin lesions elicited in C57BL/6 mice³⁴ and in BALB/c mice.²⁶ Our results on the thickness data of normal epidermis and SC are strikingly similar to those obtained by the Ti:sapphire laser-based multiphoton microscopy.⁵⁸ Here we demonstrated that increased cellular infiltration within the epidermis can be readily assessed by the noninvasive THG imaging. Although the Cr:forsterite fs laser-based multimodality nonlinear microscopy can provide subcellular resolution and histological features without using exogenous markers,²³ the appropriate use of some molecular probes for specific labeling of surface/intracellular molecules of effector cells could result in better resolution of cellular morphology and/or interaction.

The present study shows that the accuracy (validated by being comparable to histological findings) and reliability (consistent and reproducible results in the murine model and AD patients) of Cr:forsterite fs laser-based nonlinear micros-

copy make it a facile and appropriate diagnostic and monitoring technique for AD. Intravital applications of *in vivo* and real-time imaging techniques will allow clinicians to investigate the real molecular events and cellular behavior of immune response under physiological condition.⁶ We predict that Cr:forsterite fs laser-based nonlinear microscopy probably will revolutionize the understanding of AD via glimpses through an optical window into real-life behavior of immune cells. We wish to further refine this tool for the study of human AD and eventually to other diseases, such as psoriasis.

Acknowledgment

The authors would like to acknowledge the support from the National Science Council of Taiwan under NSC 97-2314-B-002-074 -MY2, National Health Research Institute of Taiwan under NHRI-EX97-9201EI, and the NTU Research Center for Medical Excellence.

References

1. D. Y. M. Leung and T. Bieber, "Atopic dermatitis," *Lancet* **361**, 151–160 (2003).
2. E. B. Mitchell, J. Crow, G. Williams, and T. A. Platts-Mills, "Increase in skin mast cells following chronic house dust mite exposure," *Br. J. Dermatol.* **114**, 65–73 (1986).
3. N. Novak, T. Bieber, and D. Y. M. Leung, "Immune mechanisms leading to atopic dermatitis," *J. Allergy Clin. Immunol.* **112**, S128–139 (2003).
4. D. Y. M. Leung, "Atopic dermatitis: the skin as a window into the pathogenesis of chronic allergic diseases," *J. Allergy Clin. Immunol.* **96**, 302–318 (1995).
5. P. O. Fiset, D. Y. M. Leung, and Q. Hamid, "Immunopathology of atopic dermatitis," *J. Allergy Clin. Immunol.* **118**, 287–290 (2006).
6. H. H. Radeke, R. J. Ludwig, and W. H. Boehncke, "Experimental approaches to lymphocyte migration in dermatology *in vitro* and *in vivo*," *Exp. Dermatol.* **14**, 641–666 (2005).
7. C. Sumen, T. R. Mempel, I. B. Mazo, and U. H. von Andrian, "Intravital microscopy: visualizing immunity in context," *Immunity* **21**, 315–329 (2004).
8. B. R. Masters, P. T. So, K. H. Kim, C. Buehler, and E. Gratton, "Multiphoton excitation microscopy, confocal microscopy, and spectroscopy of living cells and tissues; functional metabolic imaging of human skin *in vivo*," *Methods Enzymol.* **307**, 513–536 (1999).
9. M. J. Koehler, K. König, P. Elsner, R. Buckle, and M. Kaatz, "In vivo assessment of human skin aging by multiphoton laser scanning tomography," *Opt. Lett.* **31**, 2879–2881 (2006).
10. K. König and I. Riemann, "High-resolution multiphoton tomography of human skin with subcellular spatial resolution and picosecond time resolution," *J. Biomed. Opt.* **8**, 432–439 (2003).
11. U. K. Tirlapur, K. König, C. Peuckert, R. Krieg, and K. J. Halbhauer, "Femtosecond near-infrared laser pulses elicit generation of reactive oxygen species in mammalian cells leading to apoptosis-like death," *Exp. Cell Res.* **263**, 88–97 (2001).
12. G. J. Tearney, M. E. Brezinski, B. E. Bouma, S. A. Boppart, C. Pitris, J. F. Southern, and J. G. Fujimoto, "In vivo endoscopic optical biopsy with optical coherence tomography," *Science* **276**, 2037–2039 (1997).
13. S. W. Chu, S. Y. Chen, T. H. Tsai, T. M. Liu, C. Y. Lin, H. J. Tsai, and C. K. Sun, "In vivo developmental biology study using noninvasive multi-harmonic generation microscopy," *Opt. Express* **11**, 3093–3099 (2003).
14. C. K. Sun, S. W. Chu, S. Y. Chen, T. H. Tsai, T. M. Liu, C. Y. Lin, and H. J. Tsai, "Higher harmonic generation microscopy for developmental biology," *J. Struct. Biol.* **147**, 19–30 (2004).
15. S. Y. Chen, C. S. Hsieh, S. W. Chu, C. Y. Lin, C. Y. Ko, Y. C. Chen, H. J. Tsai, C. H. Hu, and C.-K. Sun, "Noninvasive harmonics optical microscopy for long-term observation of embryonic nervous system development *in vivo*," *J. Biomed. Opt.* **11**, 054022 (2006).
16. C. S. Hsieh, S. U. Chen, Y. W. Lee, Y. S. Yang, and C. K. Sun, "Higher harmonic generation microscopy of *in vitro* cultured mammal oocytes and embryos," *Opt. Express* **16**, 11574–11588 (2008).

17. K. König, P. T. So, W. W. Mantulin, and E. Gratton, "Cellular response to near-infrared femtosecond laser pulses in two-photon microscopes," *Opt. Lett.* **22**, 135–136 (1997).
18. J. M. Squirrell, D. L. Wokosin, J. G. White, and B. D. Bavister, "Long-term two-photon fluorescence imaging of mammalian embryos without compromising viability," *Nat. Biotechnol.* **17**, 763–767 (1999).
19. American National Standards Institute (ANSI), *American National Standard for Safe Use of Lasers, Z136.1*, Laser Institute of America, Orlando, FL (2007).
20. S. Parker, "Laser regulation and safety in general dental practice," *Br. Dent. J.* **202**, 523–532 (2007).
21. C. K. Sun, C. C. Chen, S. W. Chu, T. H. Tsai, Y. C. Chen, and B. L. Lin, "Multiharmonic-generation biopsy of skin," *Opt. Lett.* **28**, 2488–2490 (2003).
22. S. P. Tai, T. H. Tsai, W. J. Lee, D. B. Shieh, Y. H. Liao, H. Y. Huang, K. Zhang, H. L. Liu, and C. K. Sun, "Optical biopsy of fixed human skin with backward-collected optical harmonics signals," *Opt. Express* **13**, 8231–8242 (2005).
23. C. K. Sun, "Higher harmonic generation microscopy," *Adv. Biochem. Eng./Biotechnol.* **95**, 17–56 (2005).
24. K. Schenke-Layland, I. Riemann, O. Damour, U. A. Stock, and K. König, "Two-photon microscopes and *in vivo* multiphoton tomographs—powerful diagnostic tools for tissue engineering and drug delivery," *Adv. Drug Delivery Rev.* **58**, 878–896 (2006).
25. C. H. Yu, S. P. Tai, C. T. Kung, I. J. Wang, H. C. Yu, H. J. Huang, W. J. Lee, Y. F. Chan, and C. K. Sun, "*In vivo* and *ex vivo* imaging of intra-tissue elastic fibers using third-harmonic-generation microscopy," *Opt. Express* **15**, 11167–11177 (2007).
26. J. M. Spergel, E. Mizoguchi, H. Oettgen, A. K. Bhan, and R. S. Geha, "Roles of TH1 and TH2 cytokines in a murine model of allergic dermatitis," *J. Clin. Invest.* **103**, 1103–1111 (1999).
27. L. F. Wang, J. Y. Lin, K. H. Hsieh, and R. H. Lin, "Epicutaneous exposure of protein antigen induces a predominant TH2-like response with high IgE production in mice," *J. Immunol.* **156**, 4077–4082 (1996).
28. T. Y. F. Tsang, "Optical third-harmonic generation at interfaces," *Phys. Rev. A* **52**, 4116–4125 (1995).
29. F. Fine and W. P. Hansen, "Optical second harmonic generation in biological systems," *Appl. Opt.* **10**, 2350–2353 (1971).
30. D. Débarre, A. M. Pena, W. Supatto, T. Boulesteix, M. Strupler, M. P. Sauviat, J. L. Martin, M. C. Schanne-Klein, and E. Beaupaire, "Second- and third-harmonic generation microscopies for the structural imaging of intact tissues," *Med. Sci. (Paris)* **22**, 845–850 (2006).
31. D. Yelin and Y. Silberberg, "Laser scanning third-harmonic-generation microscopy in biology," *Opt. Express* **5**, 169–175 (1999).
32. S. P. Tai, W. J. Lee, D. B. Shieh, P. C. Wu, H. Y. Huang, C. H. Yu, and C. K. Sun, "*In vivo* optical biopsy of hamster oral cavity with epi-third-harmonic-generation microscopy," *Opt. Express* **14**, 6178–6187 (2006).
33. Y. T. Lin, C. T. Wang, J. H. Lee, C. Y. Chu, W. C. Tsao, Y. H. Yang, and B. L. Chiang, "Higher Bcl-2 levels decrease staphylococcal superantigen-induced apoptosis of CD4+T cells in atopic dermatitis," *Allergy* **62**, 520–526 (2007).
34. J. M. Spergel, E. Mizoguchi, J. P. Brewer, T. R. Martin, A. K. Bhan, and R. S. Geha, "Epicutaneous sensitization with protein antigen induces localized allergic dermatitis and hyperresponsiveness to methacholine after single exposure to aerosolized antigen in mice," *J. Clin. Invest.* **101**, 1614–1622 (1998).
35. T. H. Tsai, S. P. Tai, W. J. Lee, H. Y. Huang, Y. H. Liao, and C. K. Sun, "Optical signal degradation study in fixed human skin using confocal microscopy and higher-harmonic optical microscopy," *Opt. Express* **14**, 749–758 (2006).
36. E. Candi, R. Schmidt, and G. Melino, "The cornified envelope: a model of cell death in the skin," *Nat. Rev. Mol. Cell Biol.* **6**, 328–340 (2005).
37. T. Gambichler, G. Moussa, M. Sand, D. Sand, A. Orlikov, P. Altmeyer, and K. Hoffmann, "Correlation between clinical scoring of allergic patch test reactions and optical coherence tomography," *J. Biomed. Opt.* **10**, 064030 (2005).
38. M. Mogensen, H. A. Morsy, L. Thrane, and G. B. Jemec, "Morphology and epidermal thickness of normal skin imaged by optical coherence tomography," *Dermatology (Basel, Switz.)* **217**, 14–20 (2008).
39. T. Gambichler, G. Moussa, M. Sand, D. Sand, P. Altmeyer, and K. Hoffmann, "Applications of optical coherence tomography in dermatology," *J. Dermatol. Sci.* **40**, 85–94 (2005).
40. K. S. Nehal, D. Gareau, and M. Rajadhyaksha, "Skin imaging with reflectance confocal microscopy," *Semin Cutan Med. Surg.* **27**, 37–43 (2008).
41. S. González, E. González, W. M. White, M. Rajadhyaksha, and R. R. Anderson, "Allergic contact dermatitis: correlation of *in vivo* confocal imaging to routine histology," *J. Am. Acad. Dermatol.* **40**, 708–713 (1999).
42. S. Astner, S. González, and E. Gonzalez, "Noninvasive evaluation of allergic and irritant contact dermatitis by *in vivo* reflectance confocal microscopy," *Contact Dermatitis* **17**, 182–191 (2006).
43. P. T. C. So, C. Y. Dong, B. R. Masters, and K. M. Berland, "Two-photon excitation fluorescence microscopy," *Annu. Rev. Biomed. Eng.* **2**, 399–429 (2000).
44. M. Oheim, D. J. Michael, M. Geisbauer, D. Madsen, and R. H. Chow, "Principles of two-photon excitation fluorescence microscopy and other nonlinear imaging approaches," *Adv. Drug Delivery Rev.* **58**, 788–808 (2006).
45. I. H. Chen, S. W. Chu, C. K. Sun, P. C. Cheng, and B. L. Lin, "Wavelength dependent damage in biological multiphoton confocal microscopy: a micro-spectroscopic comparison between femtosecond Ti:sapphire and Cr:forsterite laser sources," *Opt. Quantum Electron.* **34**, 1251–1266 (2002).
46. T. M. Liu, S. W. Chu, C. K. Sun, B. L. Lin, P. C. Cheng, and I. Johnson, "Multiphoton confocal microscopy using a femtosecond Cr:Forsterite laser," *Scanning* **23**, 249–254 (2001).
47. W. R. Zipfel, R. M. Williams, and W. W. Webb, "Nonlinear magic: multiphoton microscopy in the biosciences," *Nat. Biotechnol.* **21**, 1369–1377 (2003).
48. R. R. Anderson and J. A. Parrish, "The optics of human skin," *J. Invest. Dermatol.* **77**, 13–19 (1981).
49. T. J. McIntosh, "Organization of skin stratum corneum extracellular lamellae: diffraction evidence for asymmetric distribution of cholesterol," *Biophys. J.* **85**, 1675–1681 (2003).
50. A. Pena, M. Strupler, T. Boulesteix, and M. Schanne-Klein, "Spectroscopic analysis of keratin endogenous signal for skin multiphoton microscopy," *Opt. Express* **13**, 6268–6274 (2005).
51. J. A. Palero, H. S. de Bruijn, A. van der Ploeg van den Heuvel, H. J. Sterenberg, and H. C. Gerritsen, "Spectrally resolved multiphoton imaging of *in vivo* and excised mouse skin tissues," *Biophys. J.* **93**, 992–1007 (2007).
52. D. C. G. de Veld, T. C. Bakker Schut, M. Skurichina, M. J. Witjes, J. E. Van der Wal, J. L. Roodenburg, and H. J. Sterenberg, "Autofluorescence and Raman microspectroscopy of tissue sections of oral lesions," *Lasers Med. Sci.* **19**, 203–209 (2005).
53. S. V. Zabolotnov, A. B. Fedotov, S. O. Konorov, T. V. Veselova, I. E. Smirnova, P. K. Kashkarov, and A. M. Zheltikov, "Effective-medium-controlled third-harmonic generation in lamellar-nonuniform porous glass," *Opt. Commun.* **229**, 397–402 (2004).
54. D. Débarre, W. Supatto, A. M. Pena, A. Fabre, T. Tordjmann, L. Combettes, M. C. Schanne-Klein, and E. Beaupaire, "Imaging lipid bodies in cells and tissues using third-harmonic generation microscopy," *Nat. Methods* **3**, 47–53 (2006).
55. D. Weedon, "The spongiotic reaction pattern," Chap. 5 in *Skin Pathology*, D. Weedon, Ed., pp. 109–110, Elsevier Limited, Oxford (2002).
56. A. Zoumi, A. Yeh, and B. J. Tromberg, "Imaging cells and extracellular matrix *in vivo* by using second-harmonic generation and two-photon excited fluorescence," *Proc. Natl. Acad. Sci. U.S.A.* **99**, 11014–11019 (2002).
57. J. Gutermuth, M. Ollert, J. Ring, H. Behrendt, and T. Jakob, "Mouse models of atopic eczema critically evaluated," *Int. Arch. Allergy Immunol.* **135**, 262–276 (2004).
58. W. J. Mulholland, E. A. Arbuthnott, B. J. Bellhouse, J. F. Cornhill, J. M. Austyn, M. A. Kendall, Z. Cui, and U. K. Tirlapur, "Multiphoton high-resolution 3D imaging of Langerhans cells and keratinocytes in the mouse skin model adopted for epidermal powdered immunization," *J. Invest. Dermatol.* **126**, 1541–1548 (2006).